Robotica (2012) volume 30, pp. 79–89. © Cambridge University Press 2011
doi:10.1017/S0263574711000373

Abigaille II: toward the development of a spider-inspired climbing robot

Yasong Li†, Ausama Ahmed†, Dan Sameoto†,‡ and Carlo Menon†,*

†*Menrva Group, School of Engineering Science, Simon Fraser University, Canada*
‡*Department of Mechanical Engineering, University of Alberta, Canada*

(Received in Final Form: March 22, 2011. First published online: April 26, 2011)

SUMMARY
This paper presents a novel robotic platform, Abigaille II, designed to climb vertical surfaces using dry adhesion. Abigaille II is a lightweight hexapod prototype actuated by 18 miniaturized motors. The robot's feet consist of adhesive patches, which have microhairs with mushroom-shaped caps fixed on the top of millimeter-scale flexible posts. A pentapedal gait is used to climb flat vertical surfaces as this gait maximizes the number of legs in contact to the surface. Abigaille can however also walk by using other gaits, including the tripod gait.

KEYWORDS: Biomimetic robots; Mechatronic systems; Design; Legged robots; Climbing robot.

1. Introduction

There is evidence that geckos[1] and some species of spiders[2] are able to climb almost any surface by taking advantage of their *dry* adhesives, which rely primarily on Van der Waals forces.[3] Dry adhesion has been investigated in depth in the last decade[4–6] and engineers and physicists studied different micro/nano designs[7–9] and developed different fabrication methodologies[10–15] for obtaining synthetic versions of dry adhesives. These adhesives could potentially enable the development of climbing robots for surveillance, security, rescue, and maintenance operations in hazardous environments. Toward this goal, different climbing prototypes relying on dry adhesion have recently been proposed including robots based on wheeled locomotion systems[16–18] and inspired by the locomotion of geckos.[19–22]

On the basis of our preliminary attempts[23,24] and theoretical works proposed in recent years,[25–29] this paper presents the design and performance of a novel lightweight hexapod prototype capable of climbing vertical surfaces by using dry adhesives.

This paper is organized as follows: Section 2 presents the adhesive features and manufacturing procedure; Section 3 presents the robot's design; Section 4 investigates the potentially optimum configurations of the robot; Section 5 discusses experimental climbing tests; Section 6 presents results obtained by measuring the forces exerted by the robot at each step; Section 7 summarizes the overall performance of the robot and suggests future research directions; and Section 8 draws the conclusions of the work.

* Corresponding author. E-mail: cmenon@sfu.ca

2. Dry Adhesives with Hierarchical Structure

The feet of Abigaille II consist of a two-layer adhesive, which was manufactured in two steps. First, a $1 \times 3\text{cm}^2$ layer with microposts was manufactured[10] by casting Polydimethylsiloxane (PDMS), specifically Sylgard 184® from Dow Corning, in a microstructured mold. The mold was fabricated by spinning polymethylglutarimide (PMGI) and AZ 9260 photoresist in succession on a chrome/gold-coated silicon wafer, then developing the microholes following exposure. The PMGI was undercut from the photoresist using a timed development, leaving holes suitable for casting mushroom-shaped fibers. Figure 1 shows the scanning electron microscope (SEM) images of the microposts in the adhesive used on the climbing robot.

The second layer consisted of a $1 \times 1\text{cm}^2$ macroposts array. Each post had about 1mm^2 cross-section area and was approximately 3 mm tall. To manufacture this second layer, a Polymethyl methacrylate (PMMA) mold was fabricated by using CO_2 laser cutting technology (Universal Laser Systems VLS3.60). A cotton cloth was embedded in the PDMS while it was curing to strengthen the adhesive backing (Fig. 2). After demolding the macrofibers from the PMMA mold, they were dipped into uncured PDMS and subsequently placed on top of the first adhesive layer with microhairs to cure and glue the two fiber layers together. The manufacturing process is schematically summarized in Fig. 3.

Once the two-layer adhesive was manufactured, it was fixed to the tip of the robot's leg at a 20° angle (see Fig. 4). The macrolayer was of critical importance as it acted as compliant spherical joint and also damped down vibrations generated during the robot's locomotion; it should be noted that vibrations are one of the most important cause of detachment during vertical climbing.

3. Robot's Design

Abigaille-II has 36 degrees of freedom (DOF) of which 18 are actively controlled. A CAD model of the robot is shown in Fig. 5(b). Each leg has three revolute joints, hereafter called hip, shoulder, and elbow joints (see Fig. 5a), and one compliant ankle, which can be considered, in first approximation, as a spherical joint. The hip joint rotates about

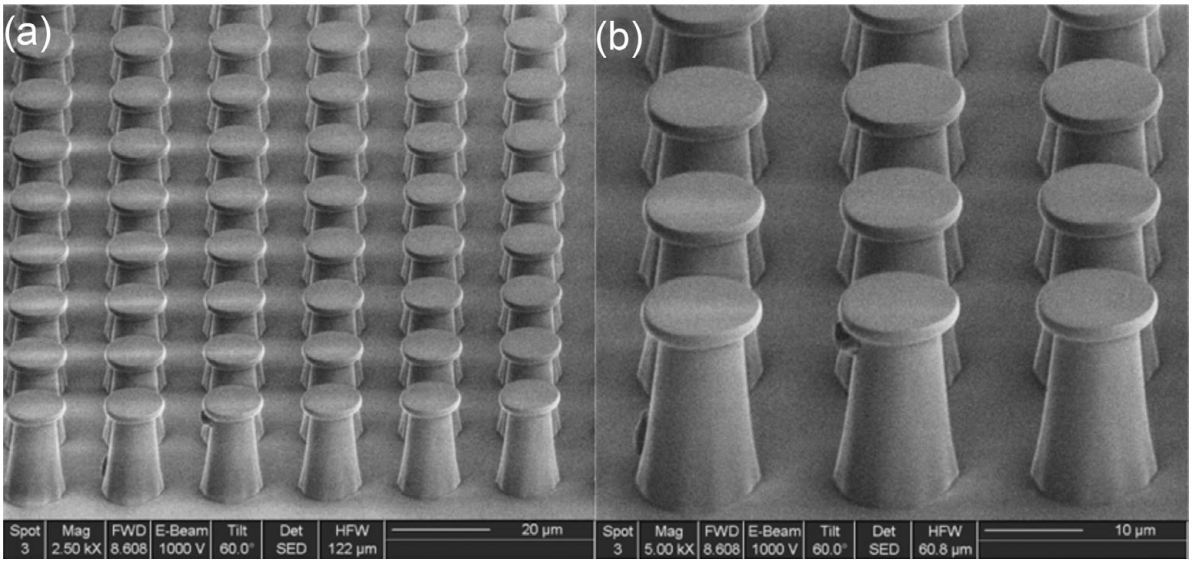

Fig. 1. SEM images of the microposts in the adhesive used in the climbing robot: (a) magnification at 2500X and (b) magnification at 5000X.

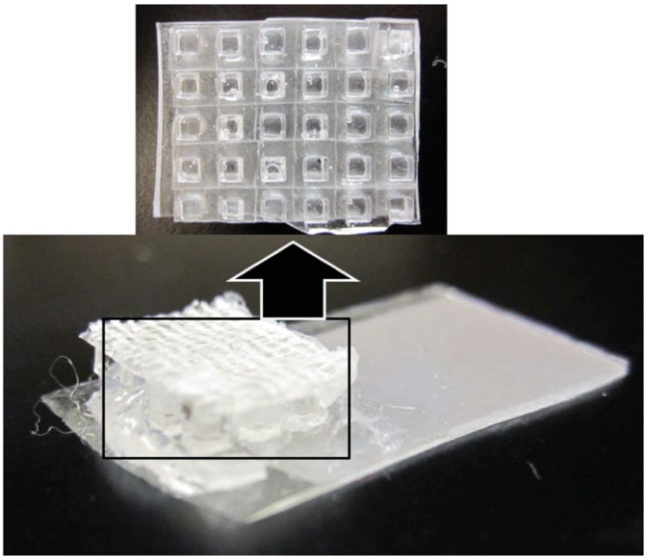

Fig. 2. (Colour online) Macroposts in the second layer of the feet.

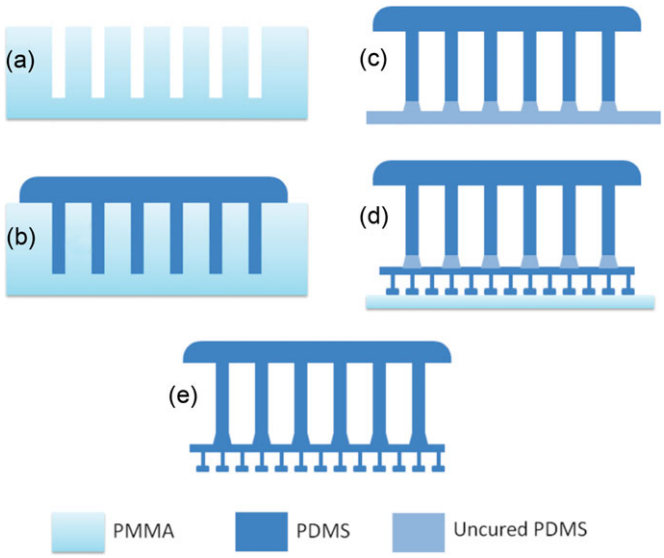

Fig. 3. (Colour online) Procedure for producing a second level hierarchal adhesive: (a) PMMA is cut using a CO_2 laser to form a pillar mold; (b) Sylgard 184 is cast and cured in the PMMA mold; (c) the demolded large pillars are dipped in uncured Sylgard 184; (d) placed on a previously cured dry adhesive sheet and cured on a low surface energy surface (PMMA); and (e) remove the final adhesive from PMMA.

the axis perpendicular to the plane defined by the body (see Fig. 5). The shoulder and elbow joints rotate instead about axes parallel to the body plane. All the legs are symmetrically arranged around the robot's body.

In order to reduce the robot's mass, its mechanical structure consists of a mosaic composition of Printed Circuit Boards (PCB) (dark gray color in Fig. 5) used to power the motors and control their angular position. The PCBs are connected together by lightweight plastic components (light gray color in Fig. 5), which were manufactured by using a rapid-prototyping machine (InVision^{TM} HR). Each revolute joint is connected to a mini gear motor GH6124S, Gizmo's Zone (black color in Fig. 5), having 6 mm diameter and a gear ratio of 1:700; maximum output torque of each motor is 200 g·cm when 3 V is supplied. The motor's shaft is fixed to the wiper back hole of a potentiometer (see Fig. 6) and the motor's body is instead connected to the potentiometer box; the extruded

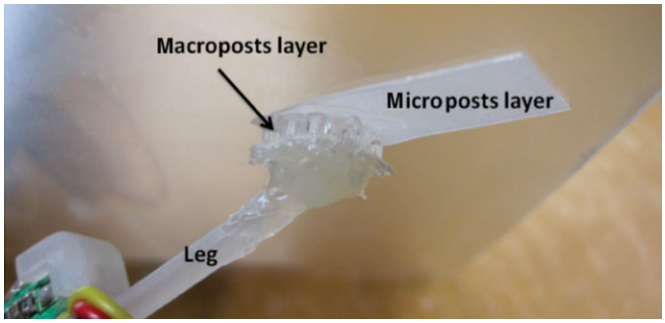

Fig. 4. (Colour online) Foot attached to a smooth surface.

https://doi.org/10.1017/S0263574711000373 Published online by Cambridge University Press

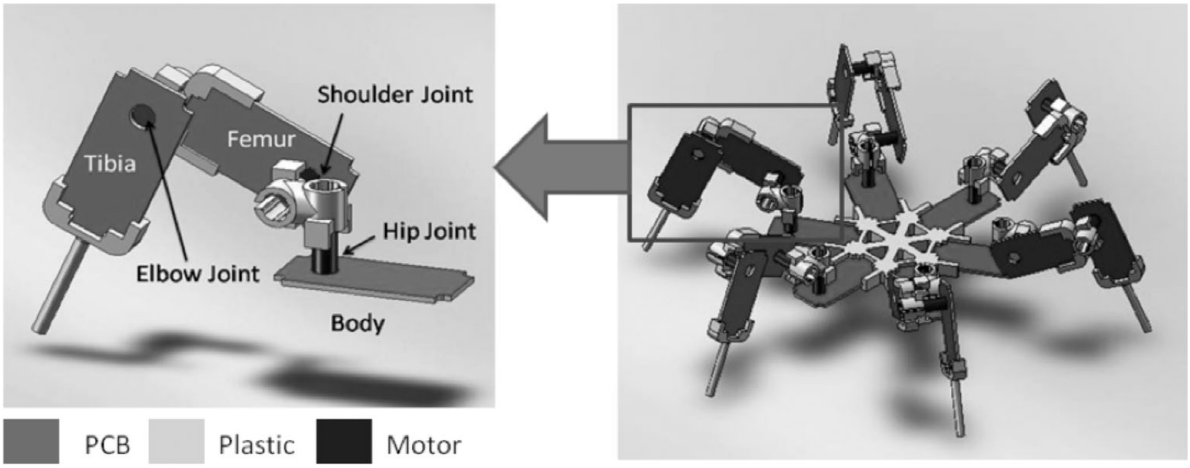

Fig. 5. (a) Leg's geometry and (b) CAD model of the robot.

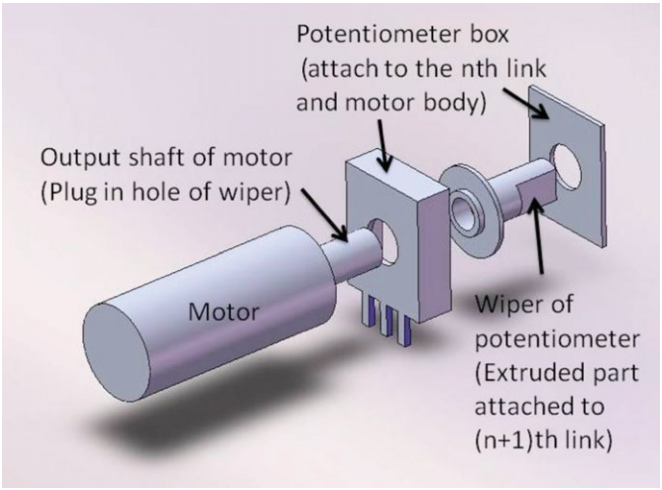

Fig. 6. (Colour online) Construction of one joint.

part from the wiper is connected to the next link, namely, to the next PCB. This compact design enables the climbing robot to have a low mass (see Table I).

A controller (SSC-32, Lynxmotion) was used to synchronize the motion of the 18 motors. Two batteries, needed to provide power both to the motors and the servo controller, were used: a 3.7 V lithium polymer battery (Sparkfun) and a 9 V rechargeable battery (Energizer). Communication between the servo controller and an external personal computer was achieved by using a Bluetooth modem (BlueSMiRF WRL-00582, Sparkfun). The external computer was used only to make the robot change gait; by using inverse kinematics equations,[23] look up tables containing trajectories for all the 18 motors were created and uploaded to the servo controller. The servo controller was wired to the 18 PCBs fixed to the motors. The servo controller could be fixed to the robot's body or could be kept separate. Figure 7 shows a schematic representation of the system, Fig. 8 shows the developed prototype on a horizontal surface, and Fig. 9 shows the developed prototype attached to a vertical Plexiglas wall. The servo controller in Fig. 9 is disconnected from the robot's body (the long, colored wires connect the motors to the servo controller) to enable the view of the 18 PCBs. The physical parameters of the prototype are summarized in Table I.

Table I. Physical parameters of robot prototype.

Robot's total weight, including servo controller and batteries	260 g
Body diameter (distance of opposite hip joints)	90 mm
Extended leg length	99 mm
Length between hip and shoulder joints (1st link)	9 mm
Femur length	34 mm
Tibia length	56 mm

4. Climbing Configuration

A quasistatic analysis was performed in order to identify the optimal configuration that the robot should have to best adhere a vertical flat surface. It is desirable to minimize the adhesive force required by any foot of the robot to prevent its detachment from the wall. Figure 10 shows a schematic representation of the robot and the notation used in the analysis. Forces acting on the robot are the gravitational force applied to the robot's center of gravity (weight of the legs is neglected) and the reaction forces applied to each foot "i", namely, F_{xi}, F_{yi} and F_{zi} (see Fig. 10). It should be noted that the reaction torques can be neglected as the connections between the adhesive pads and the legs of the robot can conveniently be modeled as spherical joints. The analysis presented in this work assumes a symmetric configuration of the robot respect to its vertical symmetric axis (namely, legs 2, 3, and 4 have symmetric positions, respectively, to legs 1, 6, and 5).

The equations of the system can be written in the following form:

$$[A][x] = [b]. \quad (1)$$

https://doi.org/10.1017/S0263574711000373 Published online by Cambridge University Press

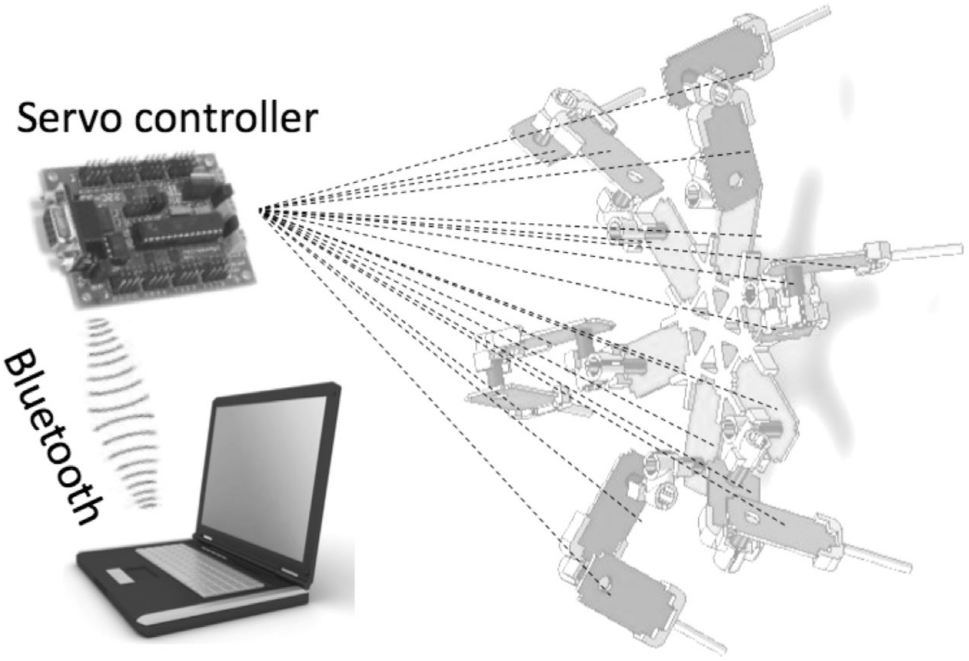

Fig. 7. Schematic representation of the system.

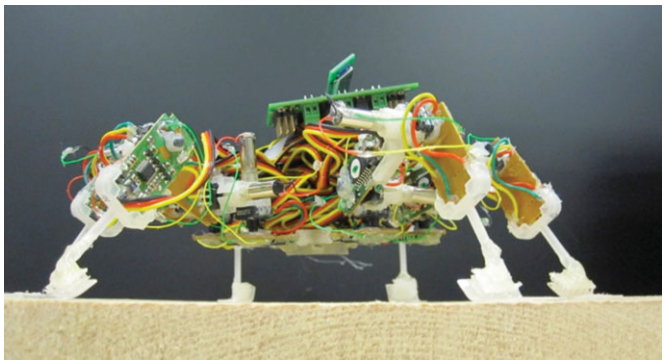

Fig. 8. (Colour online) Abigaille-II on a horizontal surface.

The vector x is the vector of the 18 unknown parameters defined as

$$[x] = [F_{x1}F_{x2}F_{x3}F_{x4}F_{x5}F_{x6}F_{y1}F_{y2}F_{y3}F_{y4}F_{y5}F_{y6}F_{z1} \times F_{z2}F_{z3}F_{z4}F_{z5}F_{z6}]^{\mathrm{T}}, \quad (2)$$

where $F_{m,n}$ are the reaction forces shown in Fig. 10, with m being the direction (x, y, z) and n the number associated to the leg (1, 2, 3, 4, 5, 6). The vector b is the vector of the forces F and torques M applied to the center of mass (CM) of the robot, namely,

$$[b] = [F_{CMx}F_{CMy}F_{CMz}M_{CMx}M_{CMy}M_{CMz}]^{\mathrm{T}}. \quad (3)$$

The matrix A is defined as

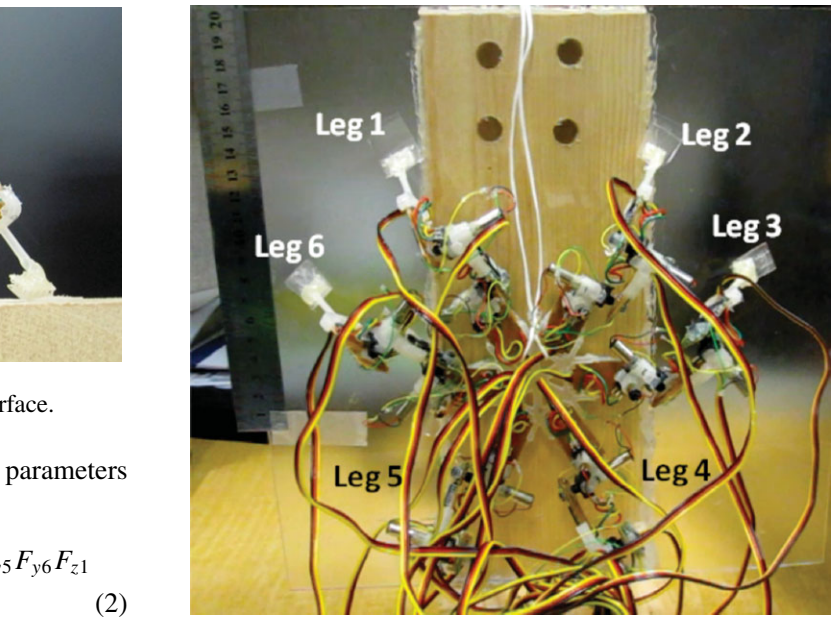

Fig. 9. (Colour online) Abigaille-II on a vertical Plexiglas wall (servo controller is not shown).

where L_{xi} and L_{yi} are the distances between the tip of each leg i and the robot's CM, respectively, along the x- and y-axes (see Fig. 11). The parameter h is the height of the robot, namely, the distance between the CM and the wall.

$$A = \begin{bmatrix} 1 & 1 & 1 & 1 & 1 & 1 & 0 & 0 & 0 & 0 & 0 & 0 & 0 & 0 & 0 & 0 & 0 & 0 \\ 0 & 0 & 0 & 0 & 0 & 0 & 1 & 1 & 1 & 1 & 1 & 1 & 0 & 0 & 0 & 0 & 0 & 0 \\ 0 & 0 & 0 & 0 & 0 & 0 & 0 & 0 & 0 & 0 & 0 & 0 & 1 & 1 & 1 & 1 & 1 & 1 \\ 0 & 0 & 0 & 0 & 0 & 0 & h & h & h & h & h & h & L_{y1} & L_{y2} & 0 & -L_{y4} & -L_{y5} & 0 \\ -h & -h & -h & -h & -h & -h & 0 & 0 & 0 & 0 & 0 & 0 & -L_{x1} & -L_{x2} & L_{x2} & L_{x4} & -L_{x5} & -L_{x6} \\ L_{y1} & -L_{y2} & 0 & L_{y4} & L_{y5} & 0 & L_{x1} & -L_{x2} & -L_{x2} & -L_{x4} & L_{x5} & L_{x6} & 0 & 0 & 0 & 0 & 0 & 0 \end{bmatrix}, \quad (4)$$

https://doi.org/10.1017/S0263574711000373 Published online by Cambridge University Press

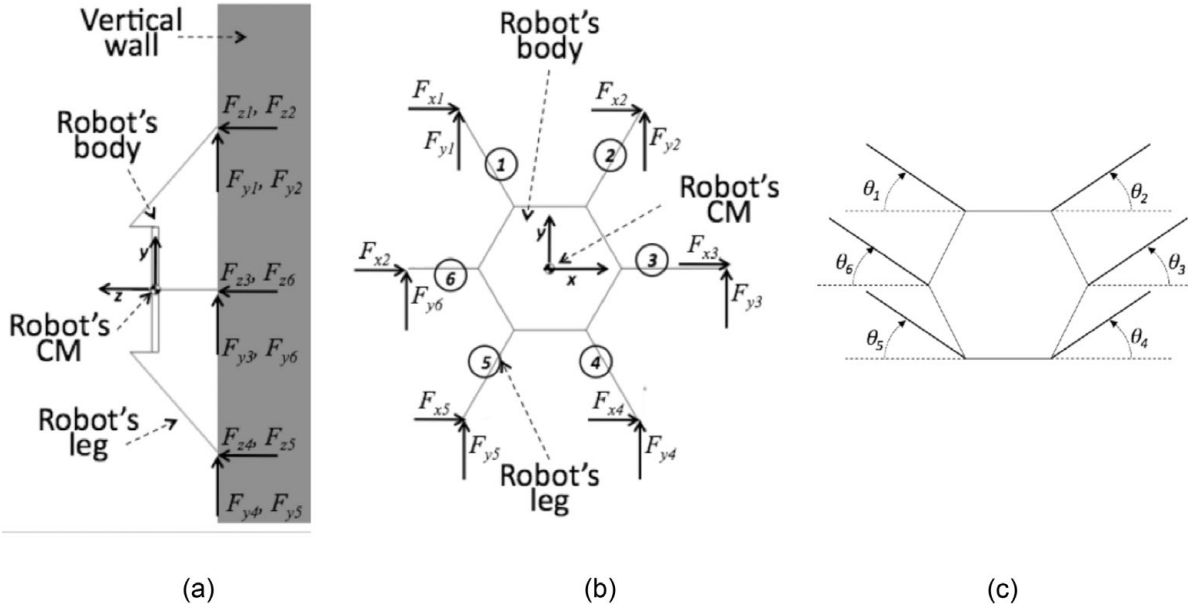

Fig. 10. Schematic representation of the robot and used notation: (a) view in the *y*--*z* plane; (b) view in the *x*–*y* plane; and (c) Positive rotation of the legs.

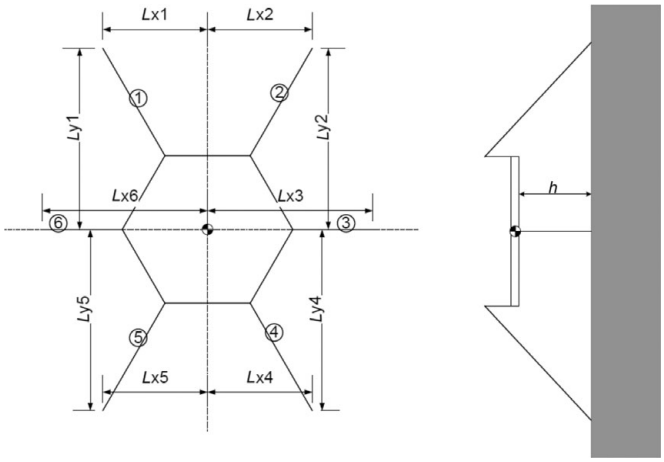

Fig. 11. Lengths nomenclature of the robot.

By considering six legs in contact with the vertical wall, Eq. (1) represents an underconstrained problem as A is rectangular matrix of dimension [6 × 18]. Among the infinite number of possible solutions, the solution of interest in this application is the one that minimizes the reaction forces at the interface between feet and vertical wall as this solution minimizes the maximum adhesion strength the feet should have (dry adhesives have in fact a practical limited adhesion strength[7]). The least square approach[30–33] was used to minimize the vector of the reaction forces for a given position of the feet; specifically, x was computed by using the right pseudoinverse as

$$[x] = [A^{\mathrm{T}}(AA^{\mathrm{T}})^{-1}][b]. \tag{5}$$

In the problem presented in this work, the only force acting on the CM of the robot was the weight of the robot itself, and therefore,

$$F_{CMx} = F_{CMz} = M_{CMx} = M_{CMy} = M_{CMz} = 0, \tag{6}$$

whereas

$$F_{CMy} = mg, \tag{7}$$

where m is the mass of the robot and g is the acceleration of gravity.

Equation (5) enables computing the optimal reaction forces for a given position of the feet of the robot. There is however the interest to also identify the optimal positions that the feet should have to minimize the adhesion forces. Figures 12–15 show the effect that the position of the feet has on the maximum reaction force. As exemplificative cases, these plots were obtained by fixing the positions of both shoulder and elbow joints of each leg and changing the rotation of the hip joints (see Fig. 5). In Figs. 12–15, the angles θ_3 and θ_6, hip joints of legs 3 and 6 (see Fig. 10), were assumed to be symmetrically equal to each other, namely, $\theta_3 = \theta_6 = \theta_{3,6}$. Similarly, the hip joints of the front legs were assumed to be symmetrically equal to each other (namely, $\theta_1 = \theta_2 = \theta_{1,2}$) and the joints of the rear legs equal to each other (namely, $\theta_4 = \theta_5 = \theta_{4,5}$). The nominal position, namely, $\theta_i = 0$, was assumed to be the horizontal position; the positive orientation of each angle is shown in Fig. 10(c). Figures 12–15 show four cases in which $\theta_{1,2} = 90$ (Fig. 12), $\theta_{1,2} = 60$ deg (Fig. 13), $\theta_{1,2} = 30$ deg (Fig. 14), and $\theta_{1,2} = 0$ deg (Fig. 15). These four figures, which parametrically show the effect of the position of the feet for a large number of configurations, outline that by bringing forward legs 1, 2, 3, and 6 (see Fig. 16) and by bringing backward the rear legs 4 and 5, the maximum reaction forces generally decreases. Figure 15 also shows that by aligning legs 1, 2, 3, and 6, the maximum reaction

https://doi.org/10.1017/S0263574711000373 Published online by Cambridge University Press

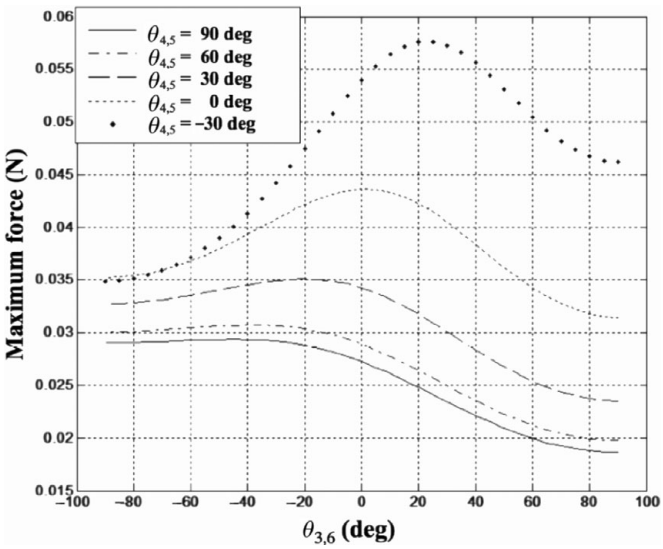

Fig. 12. Maximum reaction force when $\theta_{1,2} = 90$ deg.

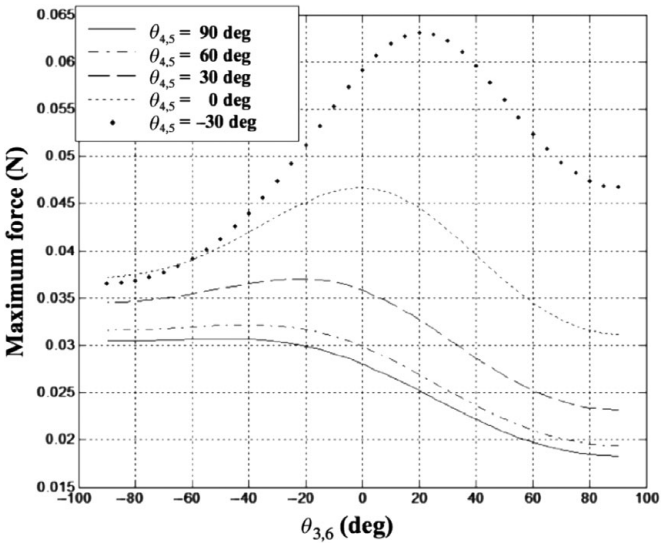

Fig. 13. Maximum reaction force when $\theta_{1,2} = 60$ deg.

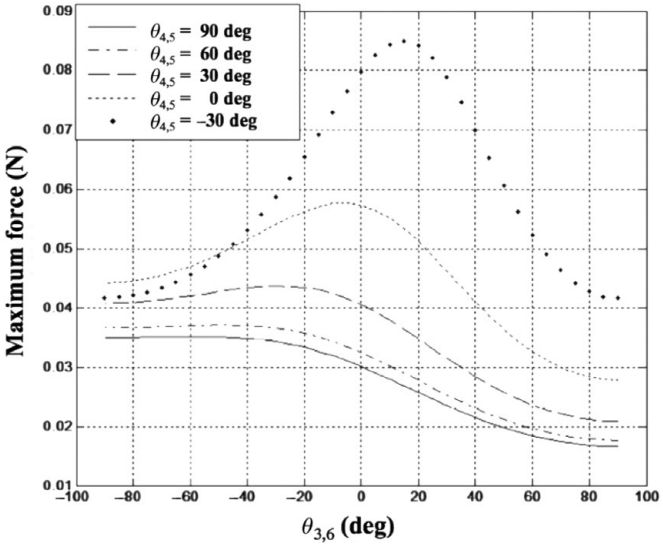

Fig. 14. Maximum reaction force when $\theta_{1,2} = 30$ deg.

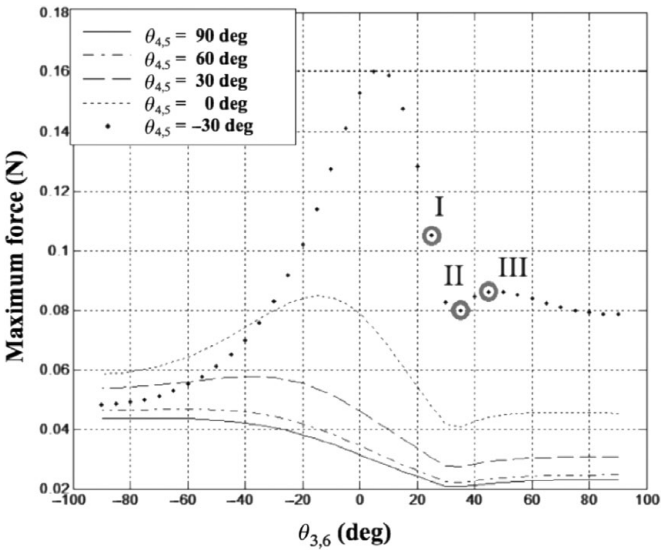

Fig. 15. Maximum reaction force when $\theta_{1,2} = 0$ deg.

force could be minimized; the variation of slope at about $\theta_{3,6} = 35$ deg is in fact caused by the legs 1 and 2 being below or above legs 3 and 6 (see Fig. 16).

In order to obtain the optimum configuration, a numerical optimization was performed based on the Genetic Algorithm.[34] In the optimization search, each foot was bounded to the space defined by the circle having the fully extended leg as radius. Each leg was assumed to be equal to each other. The configuration that minimized the reaction forces had feet 3 and 6 at the maximum upper limit in y-direction, feet 4 and 5 at their minimum lower bound in y-direction, and feet 1 and 2 in a position such that they were horizontally aligned with feet 3 and 6. It should be noted that the feet's position in x-direction does not affect the results – multiple configurations can therefore be obtained. For example, Fig. 17 shows two configurations that equivalently minimize the norm of the vector x. In these two configurations, the pulling force was equally distributed among the legs 1, 2, 3, and 6; the pushing force was instead equally distributed between the legs 4 and 5. By using the parameters of the robot presented in Table I and a height h equal to 1.5 cm, the maximum reaction force amounted to 49 mN.

We also changed the height h, while constraining the foot positions to the same search space (i.e., the projection of the fully extended legs to the vertical wall is kept constant), and recalculated the optimal foot positions. When this was done, we found that the optimal foot position in the x–y plane did not change. It is noted that the value of the maximum reaction force changed as h varied.

The conclusion of this analysis is that, while climbing a vertical surface, the robot should have a configuration close to the identified optimal configuration in order to minimize the adhesion requirements of the dry adhesive pads. It should be noted that this consideration is valid when the robot is in a steady state or moves slowly as these results were obtained through a quasistatic analysis.

https://doi.org/10.1017/S0263574711000373 Published online by Cambridge University Press

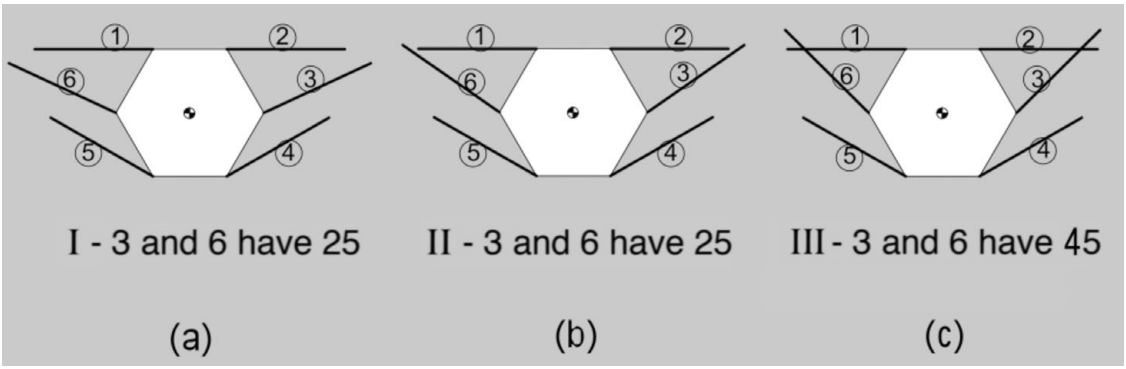

Fig. 16. Legs 3 and 6 in different positions: (a) $\theta_{3,6} = 25$ deg (see point I in Figure 15); (b) $\theta_{3,6} = 35$ deg (see point II in Figure 15); and (c) $\theta_{3,6} = 45$ deg (see point III in Figure 15).

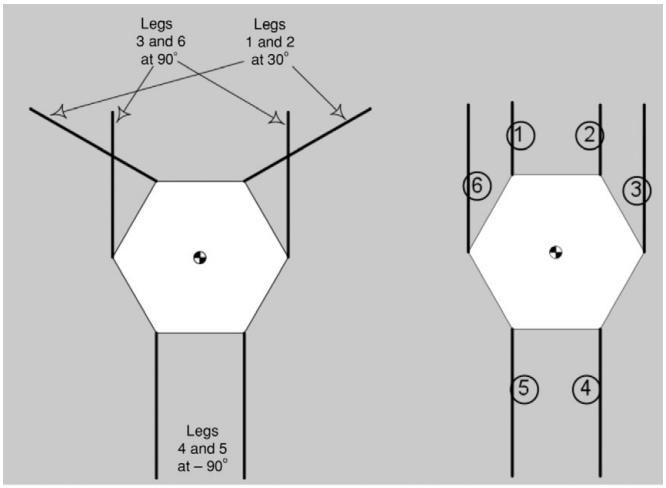

Fig. 17. Two configurations that minimize the reaction forces.

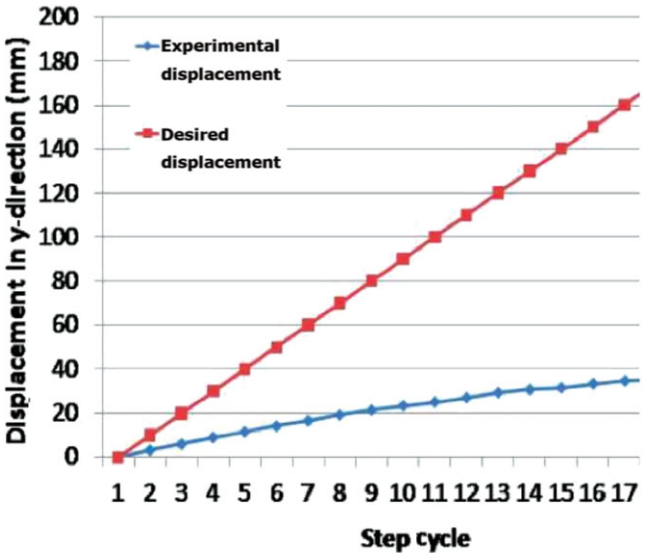

Fig. 18. (Colour online) Measurement of robot's body position on vertical wall during successive step cycles.

5. Climbing Tests

On the basis of the previous analysis, the configuration shown in Fig. 17(b) was used. In order to be close to the quasistatic conditions, and also to improve climbing robustness, the robot moved slowly, about 6 s per leg's cycle, which included the detachment, swing, and attachment phases of one robotic foot. In order to keep as many contact points as possible during vertical climbing, the pentapedal gait was selected. In this gait, legs are moved upward one at a time and the body moves at the end. The feet were detached by peeling the adhesive in order to minimize torque required by the motors – this allowed selecting very small motors. Peeling was obtained by moving each foot at a 45 deg trajectory with respect to the wall; this motion was proven to be optimum to peel compliant adhesives.[24] The trajectory to attach the adhesive was instead a straight line normal to the contacting surface – this trajectory experimentally yielded a good contact surface area between the adhesive and the vertical surface.

Abigaille II was able to climb on vertical Plexiglas surfaces. Tests were performed by video recording the robot and postprocessing the digital frames by using Vision Builder Software, National Instrument. Figure 18 shows, for example, displacement in vertical direction per step cycle. The use of kinematic equations estimated that the robot should theoretically advance about 1 cm each step. However, as shown in Fig. 18, the robot did not follow the expected prediction mainly due to the deformation of the structural frame of the robot, which was slender and flexible – when the robot lifted a leg, the other five legs bent downward, and therefore, the robot's advancement was greatly reduced.

6. Force Measurements

In order to assess the effect of the robot's dynamic motion on the adhesive's requirements, tests were performed through a customized force measurement system. Specifically, reaction forces of the feet were recorded through the use of load cells (LSM300, Futek) embedded on an instrumented vertical wall. Signals were recorded through a data acquisition board USB6008 (National Instrument). Figure 19(a)–(c) show,

https://doi.org/10.1017/S0263574711000373 Published online by Cambridge University Press

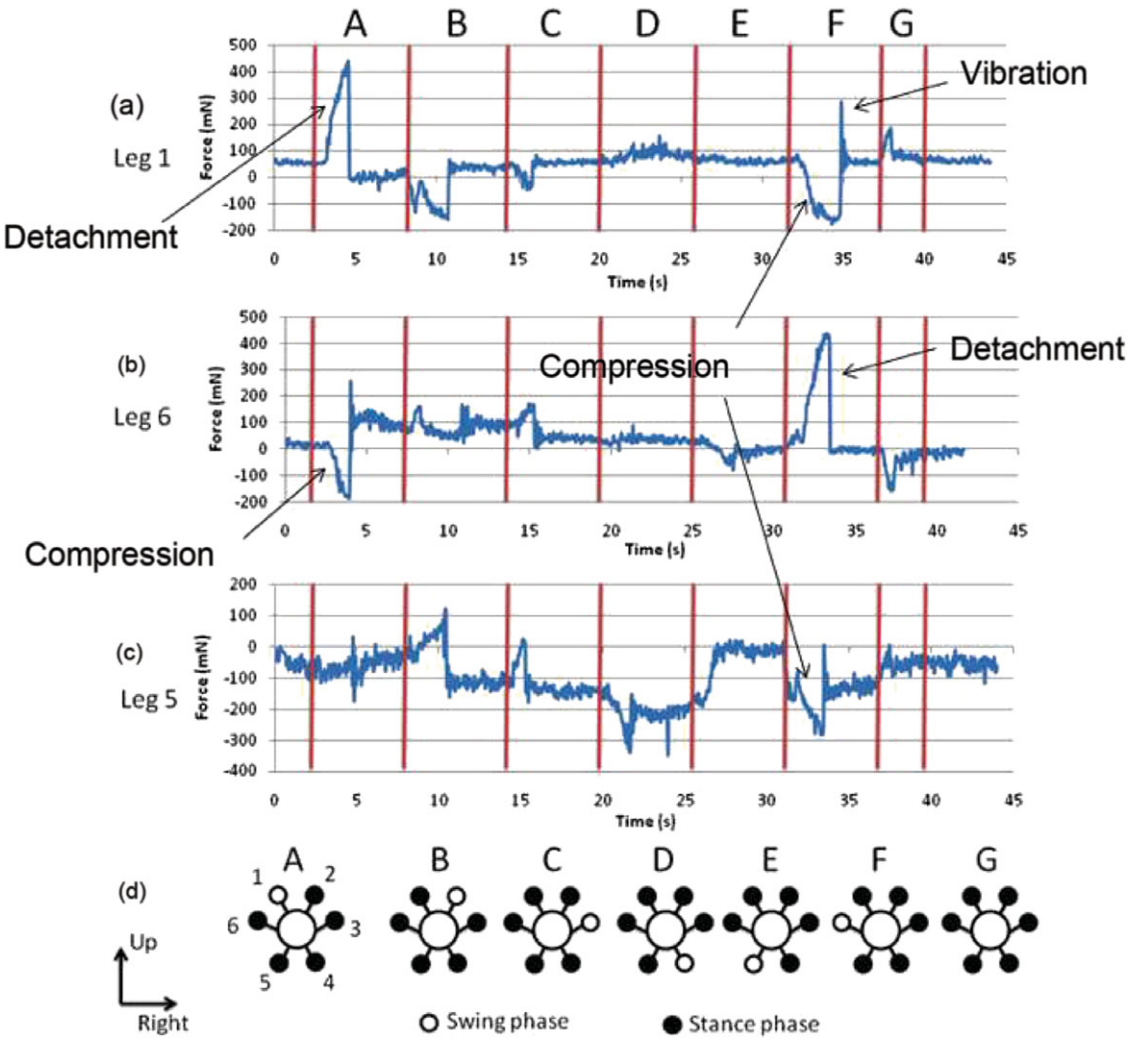

Fig. 19. (Colour online) Force characterization on legs 1, 6, and 5 during climbing: (a)–(c) force graph of legs 1, 6, and 5; and (d) Scheme of different phases in one step cycle.

respectively, the load cell output of legs 1, 6, and 5. Negative force represents compression, and positive force represents pulling force normal to the wall (the maximum pulling force sets the requirements for the adhesive). As predicted, legs 1 and 6 tend to detach from the wall while the rear legs exert compression forces against the wall for most of the time. Figure 19 is divided into seven phases, called phases A–G (Fig. 19(d)), corresponding to the six cycle steps of the six legs and the step due to the body advancement when all the legs are in contact to the wall.

Before phase A began, the robot was in a quasistatic configuration; the maximum-recorded force was about 50 ± 10 mN, which was close to the one predicted. As expected, leg 1 exerts the maximum pulling force.

An analysis of Fig. 19 leads understanding how the force is distributed during locomotion. In phase A, leg 1 detached from the surface, swung, and attached again to the surface. A force equal to 450 mN was recorded when leg 1 detached through peeling motion, (see Fig. 19a). The maximum value of this force depended mainly on the adhesive quality and size. Figure 19(b) shows that the leg 6 was compressed against the surface due to the detachment of leg 1. In phase B (see Fig. 19a), when leg 2 detached, a negative reaction force was recorded for leg 1 – therefore, leg 1 was preloaded against the wall in this phase, which helped increasing contact surface area of the adhesive. In phase C (see Fig. 19a), a similar compression force was recorded when leg 3 was peeled off the surface. In phases D and E (see Fig. 19a), namely, during the motion of the legs 4 and 2, the leg 1 reaction force was almost constant as the rear legs were relatively far away from leg 1. In phase F, leg 6 detached and, as shown in Fig. 19(b), a pulling force of about 450 mN was recorded. Leg 6 detachment caused compression of the two closest legs, namely, legs 5 (see Fig. 19c) and 1 (see Fig. 19a). It should be noted that leg 5 reattachment to the surface induced vibrations in leg 1 as shown in Fig. 19(a); this fact is particularly relevant as a peak of about 300 mN was recorded – if such a peak overcomes the strength of the adhesive (450 mN in this robot; see Fig. 19(a) phase A), the front leg detaches, and consequently, the robot may detach and fall. In phase G, all the legs are attached and the robot's base moved forward; another high peak of about 200 mN is observed in Fig. 19(a); this peak can potentially be reduced by a slower motion of the robot.

The analysis of Fig. 19 therefore shows three main features as following: (1) the robot is able to preload its feet during

https://doi.org/10.1017/S0263574711000373 Published online by Cambridge University Press

Table II. Comparison of different climbing robots relying on dry adhesives.

	Leg/ wheel	DOF (motor)	Weight (g)	Size (mm)	Steering	Transition horizontal–vertical	Corners	Any Curvature/ geometry Surface	Omni-directionality	Speed
Climbing Mini-Wheg™ [16,18]	Wheel	2 (4)	110 g/ 166.4g (no/have body joint)	Length: 89 Width: 54 Thickness:-	Yes	Yes	Yes	No	No	8.6 cm/s (60° surface, no body joint)
Waalbot[17]	Wheel	2 (2)	69 g	Length: 130 Width: 123 Thickness: 50	Yes	Yes	No	No	No	6 mm/s (straight) 37°/s (steering)
Geckobot[20]	Leg	2 (7)	100 g	Length: 190 Width: 110 Thickness:- (excluding tail)	Yes	No	No	No	No	5 cm/s (ground), 4 cm/s (tilt surface)
Stickybot[21]	Leg	38 (12)	370 g	Length: 600 Width: 200 Thickness: 60	No	No	No	No	No	24 cm/s (ground), 4 cm/s (tilt surface),
Abigaille-II	Leg	36 (18)	260 g	Body diameter: 90 Extended leg: 99	Yes	Yes	Yes	Yes	Yes	4.5 cm/s on ground (tripod gait), 0.1cm/s on vertical wall (pentapedal gait)

locomotion; (2) vibrations can easily determine adhesion failure; (3) feet close to the foot that is peeled off are the ones preloaded. These observations suggest strategies for robust locomotion. For instance, if failure of a foot is occurring, peeling motion of a closer foot could re-establish adhesion to the wall. In addition, good damping properties and smooth locomotion are essential to minimize adhesion failure during vertical climbing.

7. Overall Performance and Future Perspectives

Abigaille II demonstrated the possibility of designing a hexapod robot capable of climbing vertical surfaces relying on dry adhesion. Compared to other platforms recently developed,[16–18,20,21] the mechatronic structure of Abigaille II showed the potential of high dexterity, such as (1) turning, (2) translating in any planar direction without the need to turn, (3) rotating in-place, (4) transferring among surfaces at any slope, (5) potentially climbing and/or avoiding obstacles, and (6) locomote on surfaces of any curvature and geometry. Figure 20, for example, shows snapshots of Abigaille II while it transfers from a horizontal surface to a vertical wall.

Table II shows a comparison among different proposed climbing robots relying on dry adhesion. Abigaille II stands out as the most dexterous platform although to the cost of a high complexity of its design. It can have different gaits to cope with different scenarios; by using a tripod gait, a speed of 4.5 cm/s was, for example, reached on flat horizontal surface.

Future work would focus on different aspects to improve the robot's reliability and robustness. First, strategies to reduce adhesion failures caused by vibrations, as shown in Fig. 19, should be identified. Second, a higher control on adhesive preloading should be implemented to guarantee preloading even if the robot's structure bends under loading conditions. A potential solution would be the integration of touch sensors on the robot's feet and develop a force-feedback controller to avoid adhesion failures. Work would also focus on providing the robot with a minimum of intelligence for autonomous locomotion and path planning.

8. Conclusion

This paper presented the design and testing of a preliminary hexapod climbing prototype: Abigaille II. This prototype relies on a dual-level dry adhesive and is capable of slowly climbing a vertical flat wall and transferring between surfaces. The performed quasistatic analysis showed that the robot should have most of its legs pointing upward when standing on a vertical wall in order to minimize the adhesion strength requirements of its six adhesive pads. The force measurements that were performed provided insight on the force distribution of the forces during locomotion; it was assessed that failure mainly depends on vibrations induced at the interface between feet and wall during locomotion.

Acknowledgments

This research was supported by the European Space Agency (ESA) and the Natural Sciences and Engineering Research Council of Canada (NSERC).

https://doi.org/10.1017/S0263574711000373 Published online by Cambridge University Press

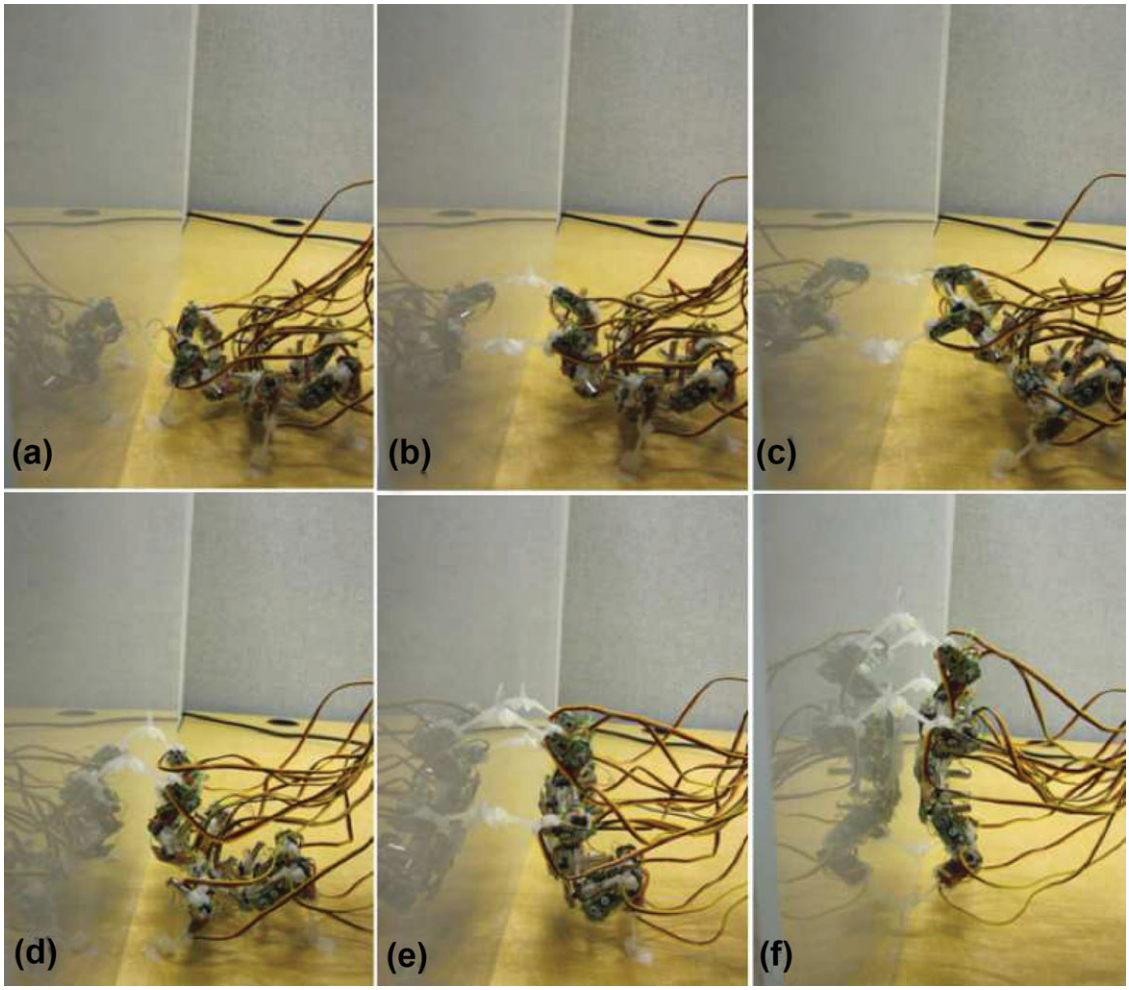

Fig. 20. (Colour online) Snap shots of robot transitioning from ground to wall.

References

1. K. Autumn, Y. Liang, T. Hsieh, W. Zesch, W. P. Chan, T. Kenny, R. Fearing and R. J. Full, "Adhesive force of a single gecko foot-hair," *Nature* **405**, 681–685 (2000).
2. A. B. Kesel, A. Martin and T. Seidl, "Getting a grip on spider attachment: An AFM approach to microstructure adhesion in arthropods," *Smart Mater. Struct*. **13**, 512–518 (2004).
3. K. Autumn, M. Sitti, Y. A. Liang, A. M. Peattie, W. R. Hansen, S. Sponberg, T. Kenny, R. Fearing, J. N. Israelachvili and R. J. Full, "Evidence for van der Waals adhesion in gecko setae," *Proc. Natl. Acad. Sci*. **99**(19), 12252–12256 (2002).
4. K. Autumn, A. Dittmore, D. Santos, M. Spenko and M. Cutkosky, "Frictional Adhesion: A new angle on gecko attachment," *J. Exp. Biol*. **209**, 3569–3579 (2006).
5. J. Lee and R. S. Fearing, "Contact self-cleaning of synthetic gecko adhesive from polymer microfibers," *Langmuir* **24**(19), 10587–10591 (2008).
6. S. Kim, E. Cheung and M. Sitti, "Wet self-cleaning of biologically inspired elastomer mushroom shaped microfibrillar adhesives," *Langmuir* **25**(13), 7196–7199 (2009).
7. D. Sameoto, Y. Li and C. Menon, "Multi-scale compliant foot designs and fabrication for use with a spider-inspired climbing robot," *J. Bionic Eng*. **5**(3), 189–196 (2008).
8. D. Sameoto, Y. Li and C. Menon, "Micromask generation for polymer morphology control: Nanohair fabrication for synthetic dry adhesives," *Adv. Sci. Technol*. **54**, 439–444 (2008).
9. D. Sameoto and C. Menon, "Direct molding of dry adhesives with anisotropic peel strength," *J. Micromech. Microeng*. **19**, 115026 (2009).
10. D. Sameoto and C. Menon, "A low-cost, high yield fabrication method for producing optimized biomimetic dry adhesives," *J. Micromech. Microeng*. **19**(11), 115002 (2009).
11. Y. Li, D. Sameoto and C. Menon, "Properties Validation of an Anisotropic Dry Adhesion Designed for Legged Climbing Robots," *Proceedings of the 2009 IEEE International Conference on Robotics and Biomimetics*, Guilin, China (2009), pp. 1906–1911.
12. J. Krahn, D. Sameoto and C. Menon, "Controllable biomimetic adhesion using embedded phase change material," *Smart Mater. Struct*. **10**(1), 015014 (2011).
13. Y. Li, D. Sameoto and C. Menon "Enhanced compliant adhesive design and fabrication with dual-level hierarchical structure," *J. Bionic Eng*. **7**(3), 228–234 (2010).
14. J. P. Díaz Téllez, C. Menon and D. Sameoto, "Cleaning properties of dry adhesives," *Sci. China Ser. E-Technological Sci*. **53**(11), 2942–2946 (2010).
15. D. Sameoto and C. Menon, "Deep UV patterning of acrylic masters for molding biomimetic dry adhesives," *J. Micromech. Microeng*. **20**(11), 115037 (2010).
16. K. A. Daltorio, S. Gorb, A. Peressadko, A. D. Horchler, R. E. Ritzmann and R. D. Quinn, "A Robot that Climbs Walls using Microstructured Polymer Feet," *Proceedings of the Eighth International Conference on Climbing and Walking Robots and the Support Technologies for Mobile Machines*, London, UK (2005) pp. 131–138.
17. M. Murphy and M. Sitti, "Waalbot: An agile small-scale wall climbing robot utilizing dry elastomer adhesives," *IEEE/ASME Trans. Mechatronics* **12**(3), 330–338 (2007).

https://doi.org/10.1017/S0263574711000373 Published online by Cambridge University Press

18. K. A. Daltorio, T. C. Witushynsky, G. D. Wile, L. R. Palmer, A. A. Malek, M. R. Ahmad, L. Southard, S. N. Gorb, R. E. Ritzmann and R. D. Quinn, "A Body Joint Improves Vertical to Horizontal Transitions of a Wall-Climbing Robot," *Proceeding of the IEEE International Conference on Intelligent Robots and Systems (ICRA '08)*, Pasadena, CA, USA (May 19–23, 2008) pp. 3046–3051.
19. C. Menon and M. Sitti, "A biomimetic climbing robot based on the Gecko," *J. Bionic Eng.* **3**(03), 115–125 (2006).
20. O. Unver, A. Uneri, A. Aydemir and M. Sitti, "Geckobot: A Gecko Inspired Climbing Robot using Elastomer Adhesives," *Proceedings of the International Conference on Robotics and Automation*, Orlando, FL, USA (2006) pp. 2329–2335.
21. S. Kim, M. Spenko, S. Trujillo, B. Heyneman, V. Mattoli and M. Cutkosky, "Whole Body Adhesion: Hierarchical, Directional and Distributed Control of Adhesion Forces for a Climbing Robot," *Proceedings of the IEEE Conference on Robotics and Automation*, Roma (2007) pp. 1268–1273.
22. C. Menon, M. Murphy and M. Sitti, "Gecko Inspired Surface Climbing Robots," *Proceedings of the IEEE International Conference on Robotics and Biomimetics*, Shenyang, China (2004) pp. 431–436.
23. C. Menon, Y. Li, D. Sameoto and C. Martens, "Abigaille-I: Towards the Development of a Spider-Inspired Climbing Robot for Space Use," *Proceedings of the 2008 2nd IEEE RAS and EMBS International Conference on Biomedical Robotics and Biomechatronics (BioRob '08)*, Scottsdale, AZ (2008) pp. 384–389.
24. Y. Li, A. Ahmed, C. Wu and C. Menon, "Preliminary Analysis of a Legged Robot Designed to Climb Vertical Surfaces," *Proceedings of the 2009 IEEE Toronto International Conference on Science and Technology for Humanity*, Toronto, Canada (2009) pp. 887–892.
25. G. Figliolini and P. Rea, "Mechanics and Simulation of Six-Legged Walking Robots," **In**: *Climbing and Walking Robots Towards New Applications* (I-Tech Education and Publishing, Austria, 2007) pp. 1–22.
26. A. Gasparetto, R. Vidoni and T. Seidl, "Passive control of attachment in legged space robots," *Appl. Bionics Biomech.*, **7**(1), 69–81 (2009).
27. A. Gasparetto and R. Vidoni, "Foot-Force Distribution and Leg Posture Analysis for a Spider-Inspired Climbing Robot," *Proceedings of the International Conference on Applied Bionics and Biomechanics (ICAAB)*, Venice, Italy (2010).
28. R. Vidoni and A. Gasparetto, "Efficient force distribution and leg posture for a bio-inspired spider robot," *J. Robot. Auton. Syst.* **59**(2), 142–150 (2011).
29. A. Gasparetto, T. Seidl and R. Vidoni, "Kinematic Study of the Spider Locomotor System in a Biomimetic Perspective," *Proceedings of the IEEE/RSJ International Conference on Intelligent Robots and Systems (IROS '08)*, Nice, France (2008) pp. 3077–3082.
30. C. D. Meyer, *Matrix Analysis and Applied Linear Algebra* (SIAM, Philadelphia, PA, USA, 2000).
31. L. Hogben, *Handbook of Linear Algebra (Discrete Mathematics and Its Applications)* (Chapman and Hall/CRC, Boca Raton, FL, USA, 2007).
32. C. L. Lawson and R. J. Hanson, *Solving Least Squares Problems* (SIAM, , Philadelphia, PA, USA, 1995).
33. R. A. Beezer, *A First Course in Linear Algebra* (Department of Mathematics and Computing Science, University of Puget Sound, Tacoma, WA, USA, 2008).
34. M. Mitchell, *An Introduction to Genetic Algorithms* (MIT Press, Cambridge, MA, USA, 1998).

https://doi.org/10.1017/S0263574711000373 Published online by Cambridge University Press